Energy & Environmental Science

Accepted Manuscript

This article can be cited before page numbers have been issued, to do this please use: X. Zhang, F. Guo, X. Jiang, A. H. Hamadamin, A. F. Lee, K. Wilson and J. Gardy, *Energy Environ. Sci.*, 2025, DOI: 10.1039/D5EE01509J.

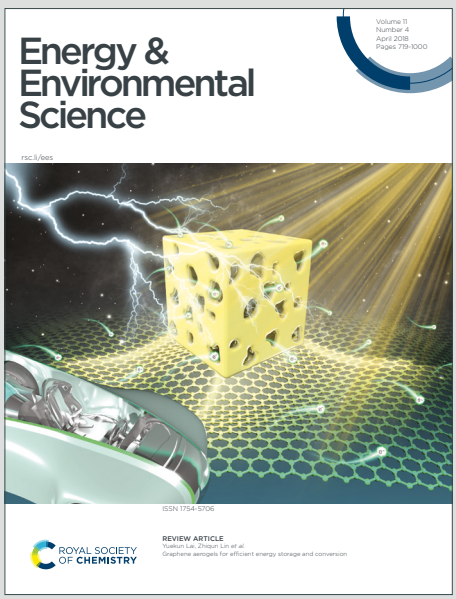

ROYAL SOCIETY OF CHEMISTRY

rsc.li/ees

View Article Online
DOI: 10.1039/D5EE01509J

Broader context statement

The global transition toward renewable energy has significantly accelerated the deployment of photovoltaic (PV) technologies. However, the rapid growth of PV power generation presents a pressing sustainability challenge: the effective end-of-life management of PV modules. Conventional recycling methods for crystalline silicon (c-Si) PV cells are hindered by high energy consumption, low material recovery efficiency, and substantial environmental impacts - factors that limit their economic and practical scalability. In this study, we introduce an innovative upcycling strategy based on Flash Joule Heating (FJH) to convert waste PV cells into high-purity silicon carbide (SiC). This ultrafast, high-temperature process enables direct and efficient synthesis of SiC by reacting silicon recovered from PV cells with carbon black, achieving >98% purity through iterative flash heating, grinding, and calcination. Compared to conventional chemical and thermal recycling methods, FJH requires 75% and 49% less energy, respectively, while reducing CO_2 emissions by 68% and 36%, respectively. These results underscore the promise of FJH as a transformative and sustainable pathway for managing silicon-based electronic waste, advancing circular economy goals, and mitigating the environmental footprint of the solar industry.

View Article Online
DOI: 10.1039/D5EE01509J

ARTICLE

Upcycling waste photovoltaic cells into silicon carbide via flash Joule heating

Ximing Zhang,[a] Feihong Guo,*[a] Xiaoxiang Jiang,*[a] Abdullah H. Hamadamin,[b] Adam. F. Lee,[c] Karen Wilson,[c] and Jabbar Gardy,[d, e]

As global demand for clean energy increases, the rapid development of photovoltaic (PV) power generation has led to a growing issue of waste PV module disposal. Traditional recycling methods face challenges such as low efficiency, high energy consumption, and environmental pollution. Flash Joule heating (FJH) technology offers a promising alternative for upcycling waste PV cells. Here, FJH was adopted to produce silicon carbide (SiC) from waste crystalline silicon (c-Si) PV cells that were pulverized and mixed with conductive carbon black (CB). Optimal reaction efficiency was achieved with an input voltage of 130 V and a peak temperature of ~2200 °C during a single flash heating cycle of 0.5 s. Repeated FJH and regrinding steps resulted in high purity SiC (>98%) after removal of excess carbon through calcination; most inorganic impurities elements were removed by evaporated during the heating process. FJH consumes significantly less energy and emits fewer greenhouse gases than alternative chemical or thermal technologies, resulting in a notable cost reduction.

Introduction

As global demand for clean energy continues to rise, photovoltaic (PV) power generation, a key component of renewable energy technologies, has experienced rapid growth[1, 2]. The global, installed capacity of PV has steadily increased, with solar energy becoming the largest source of renewable capacity in 2023, accounting for 36.7% (1418 GW). Additionally, solar energy underpinned 73% of new renewable energy installations in 2023, with global capacity projected to reach 4500 GW by 2050[3, 4]. However, a significant issue associated with this growth is the disposal of waste PV modules, which typically have a service life of ~25 years[5, 6]. It is estimated that China will generate 1.5 million tons of waste PV modules by 2030, rising to 20 million tons by 2050 (and 80 million tons globally)[7, 8].

Photovoltaic power generation technology is classified into three generations: the first comprises crystalline silicon (c-Si) cells; the second includes thin-film cells; and the third features emerging technologies such as perovskite and organic solar cells[9, 10]. The c-Si cells account for >92% of the PV market share, and are the primary component of waste PV modules[11, 12]. A typical c-Si PV module consists of glass, ethylene-vinyl acetate (EVA), c-Si cells, a backsheet, and other components in a laminated structure. Among these, glass, silicon, and metals (e.g., Ag, Al, Cu) are the primary recyclable components[13-15]. Although incineration or burial of waste modules may seem convenient, these methods release hazardous substances that can severely pollute the environment and pose health risks[16, 17]. Common methods for recycling waste PV modules include mechanical, thermal, and chemical recycling[18, 19].

Mechanical recycling involves splitting and crushing waste PV modules, separating the glass and backsheets, and grinding and sieving to recover metals and c-Si particles[20]. Thermal and chemical recycling decompose the EVA using high-temperature heating and organic solvent immersion, respectively, to separate and recover PV module components[21, 22]. While the mechanical process is (relatively) environmentally friendly and easy to operate, it has a low recovery rate and the resulting c-Si requires reprocessing. Thermal and chemical recycling achieve higher recovery rates but produce large amounts of hazardous waste gas and liquid[23-25].

Converting c-Si from waste PV modules into functional materials, such as SiC, is an attractive recycling strategy[26, 27]. Conventional SiC synthesis methods include chemical vapor deposition (CVD), self-propagation high-temperature synthesis (SHS), and Atchison carbothermal reduction (ACR). While CVD enables fine-tuning of multiple parameters, it requires expensive precursors[28]. SHS and ACR reduce feedstock costs but require lengthy processing[29, 30]. Waste PV modules provide raw materials for SiC synthesis, necessitating the development of convenient, low-energy methods.

Flash Joule heating (FJH) is a technique that uses the Joule effect to rapidly convert electrical energy into thermal energy, enabling efficient material processing[31, 32]. By applying high voltage and current, materials can be heated to temperatures

[a] Engineering Laboratory for Energy System Process Conversion and Emission Control Technology of Jiangsu Province, School of Energy and Mechanical Engineering, Nanjing Normal University, Nanjing, 210042, China.
[b] Department of Pharmaceutical Chemistry, Pharmacy College, Hawler Medical University, 44001, Erbil, Kurdistan Region, Iraq.
[c] Centre for Catalysis and Clean Energy, Griffith University, Gold Coast, QLD 4222, Australia.
[d] School of Chemical and Process Engineering, University of Leeds, LS2 7QB, Leeds, United Kingdom.
[e] Chemistry Department, College of Science, Salahaddin University-Erbil, 44002, Erbil, Iraqi Kurdistan Region.
†Electronic supplementary information (ESI).

>2900 °C in milliseconds to seconds, significantly accelerating reaction time[33] without the need for additional catalysts. FJH incurs minimal energy losses, and hence reduces overall energy consumption[34]. FJH has already found applications for the rapid synthesis of graphene from diverse carbon sources[35, 36], the recovery of precious metals and removal of hazardous heavy metals[37, 38], and the reduction and structural restoration of cathode materials[39].

In this study, we use FJH to integrate the upcycling of waste upcycling of c-Si PV cells with the synthesis of high purity SiC - a commercially valuable material widely used in abrasive machining, electrics, optics, and composite applications[40-42]. While FJH has previously been explored for the upcycling of glass fibre-reinforced plastics, this work extends its application to c-Si PV cells, involving distinct feedstocks and reaction pathways. FJH rapidly heats crushed silicon powder from waste PV modules to temperature exceeding >2000 ℃, initiating a reaction with co-mixed carbon black to form SiC while simultaneously enabling the evaporative removal of most residual metals, thereby supporting elemental circularity. This study investigates key process parameters, including applied voltage and carbon content to optimise SiC quality. In addition, we demonstrate that post-heating/regrinding enhances reaction conversion and increases product purity. The SiC derived from c-Si exhibits stable phase behaviour. Life cycle assessment and technoeconomic analysis of the FJH-based process reveal substantial cost and energy advantages over conventional recycling and upcycling methods, along with a reduced environmental footprint. This approach presents an effective route for mitigating resource demand through the sustainable upcycling of end-of-life PV modules.

Experimental

The c-Si PV cell fragments (mono-crystalline, original size: 182 mm ±0.5 × 182 mm ±0.5, Φ = 247 mm ±0.5) were first placed into a pulverizer and crushed to micron-sized powder after 5 minutes (**Figure S1**). Due to its high electrical resistance, the c-Si powder was then mixed mechanically with conductive additives in specified proportions (**Figure 1a, Table S1**). The addition of CB enhances the electrical conductivity and serves as a reactant for SiC production. The mixture of c-Si powder and CB, typically in 1:1 mass ratio, was placed into a quartz tube and manually compressed. Graphite plugs were placed at each end of the powder mixture to secure the material. The quartz tube was then positioned between two metal electrodes (one solid and the

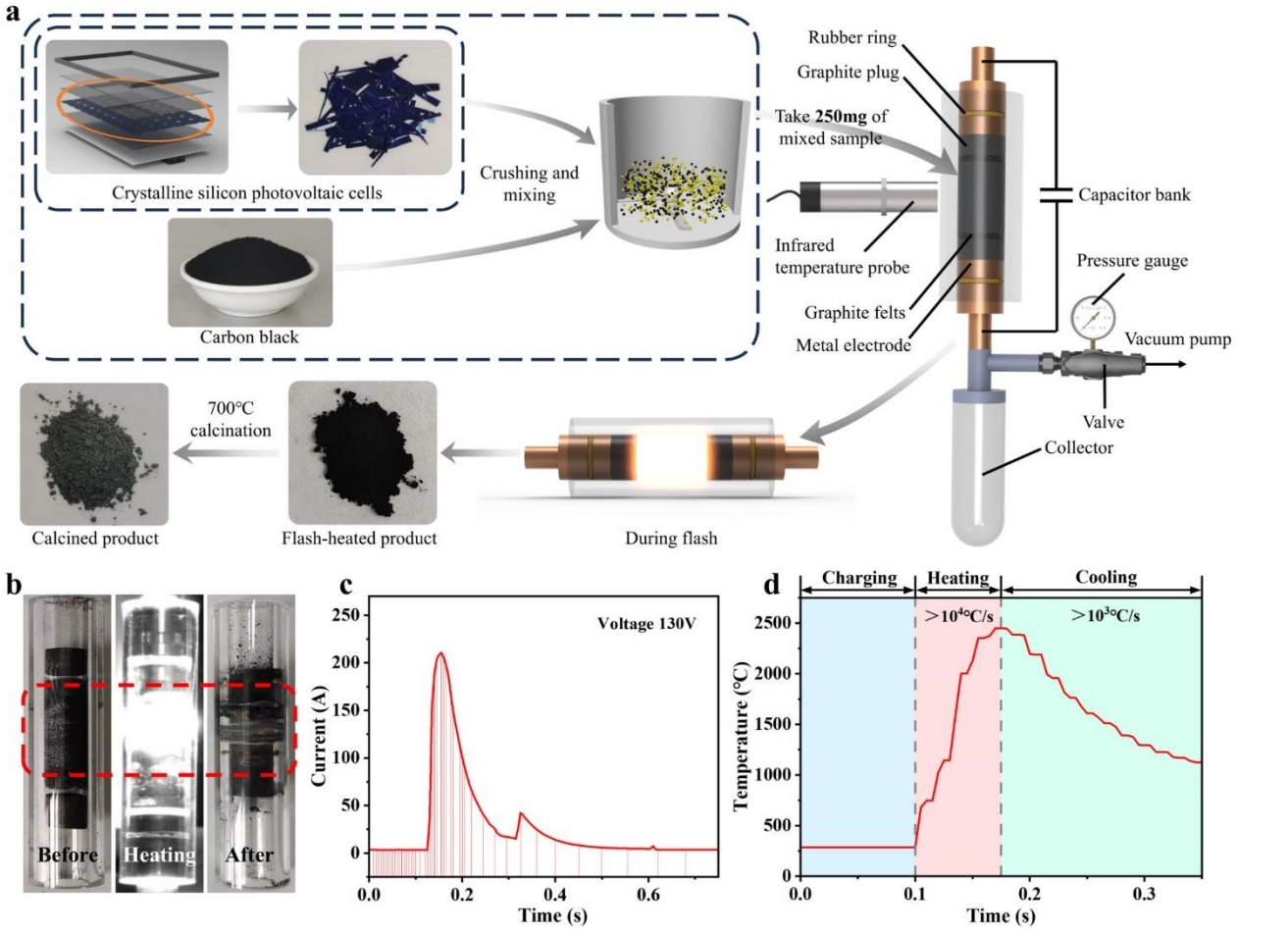

Figure 1 (a) Flowchart of the FJH experiment. (b) Comparison of the quartz tube before, during, and after FJH with sample addition. (c) Current curve at an input voltage of 130 V and a duration of 0.5 s. (d) Actual temperature curve recorded using an infrared thermometer.

other porous), with the graphite plug separating the powder from the electrodes. One side of the device was sealed with the solid electrode, with the porous electrode connected by stainless teel pipework to a sample collector, pressure gauge, and vacuum pump (for evacuation and to facilitate gas diffusion, **Figure S2**). The two electrodes were connected to a capacitor bank (total capacity 90 mF), with sample resistance adjusted by turning a screw to modify the distance between electrodes. The device was then evacuated to ~1.33 kPa, the sample resistance adjusted to ~2.5 Ω, and the desired input voltage set before charging the capacitor bank through a DC power supply. Upon discharging, the capacitor bank instantaneously released its energy, heating the sample to high temperatures within milliseconds (**Figure 1b**, **Figure S3**). Current fluctuations at different flash voltages were recorded in real time alongside temperature changes using a data acquisition system (**Figure S4**). At an input voltage of 130 V, the maximum current through the sample reached ~210 A in 0.5 s, with peak temperatures exceeding 2000 °C (**Figure 1c**). The heating rate of the FJH process was extremely rapid (>10^4 °C s^{-1}), with the peak temperature reached in < 0.1 s for various input voltages. The cooling rate (>10^3 °C s^{-1}) increased with peak temperature (**Figure 1d**). As the sample resistance was much greater than that of the graphite and metal electrodes, the voltage drop primarily occurred across the sample, consistent with simulation. This concentrates the high temperature on the sample during the FJH process. Numerical simulations indicate that the temperature distribution is relatively uniform in both the radial and longitudinal directions between the sample and the quartz

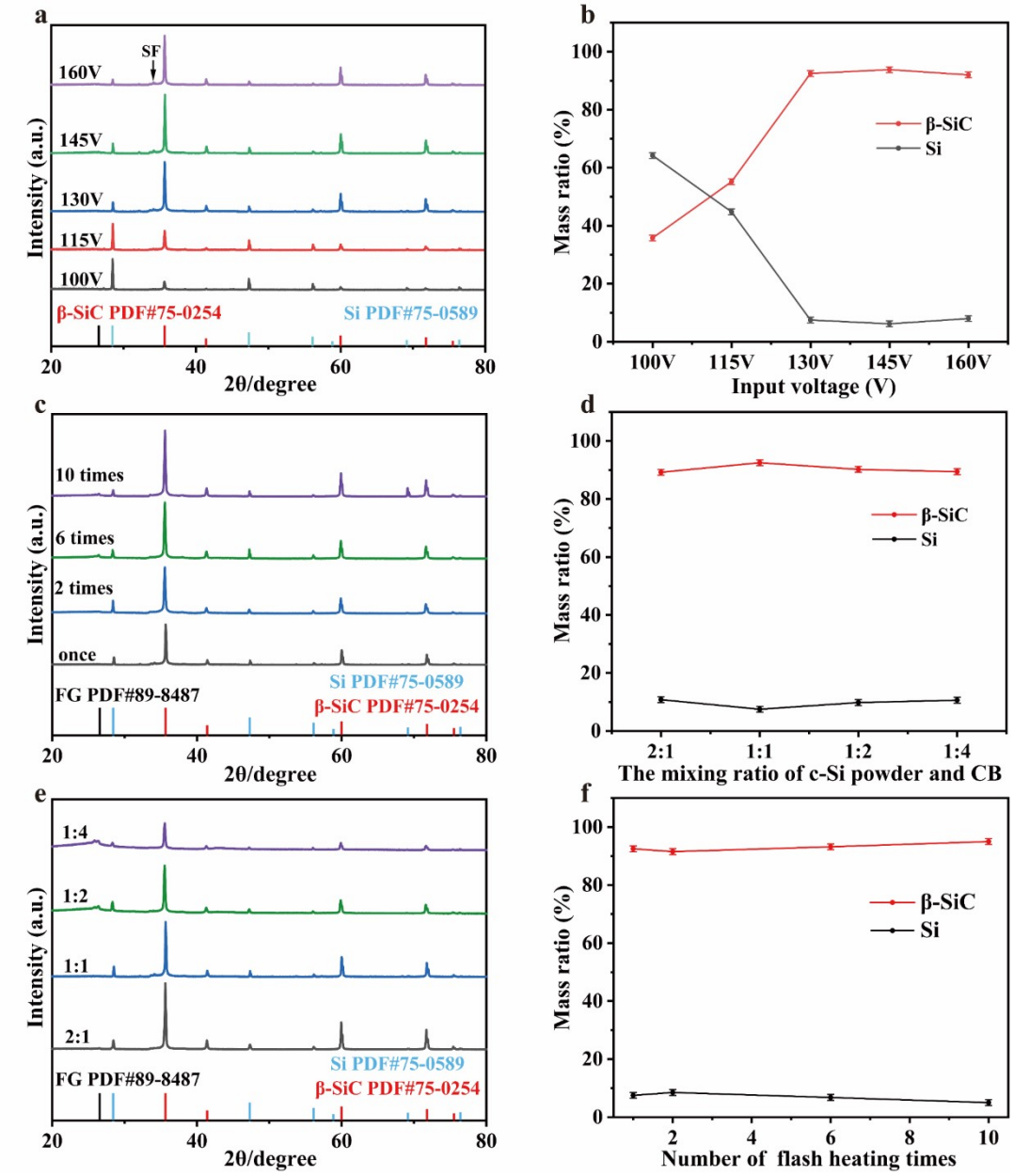

Figure 2 (a) X-ray diffractograms, and (b) composition of sold product from a single FJH cycle as a function of input voltage. (c) X-ray diffractograms, and (d) composition of solid product from a single FJH cycle as a function of c-Si powder:CB mass ratio at 130 V. (e) X-ray diffractograms, and (f) composition of solid product as a function of FJH cycles at 130 V. Standard deviation of ±1 wt %.

View Article Online DOI: 10.1039/D5EE01509J

tube (**Figure S5**). Various process parameters were explored (**Table S1**).

Results and discussion

3.1 Physicochemical properties of FJH product

Crystalline phases in the solid residue of a single FJH cycle were determined by powder X-ray diffraction for a 1:1 mass ratio of c-Si powder to CB at various input voltages (**Figure 2a**). Only silicon and cubic silicon carbide were observed; the latter being the desired product with a lattice parameter a = 4.358 Å, very similar to that reported in other studies[43, 44]. Reflections at 2θ = 35.7°, 41.4°, 60.1°, and 71.8° correspond to the (111), (200), (220), and (311) planes of β-SiC, respectively[45]. β-SiC has a cubic crystal structure[46] (**Figure S6**). A weak peak observed at 2θ = 34° may be attributed to stacking faults within β-SiC crystals[47, 48]. Reflections at 2θ = 28.5°, 47.4°, and 56.2° correspond to unreacted silicon.

FJH parameters were optimized through analysis of SiC and Si crystalline phases. For a constant sample resistance (~2.5 Ω), increasing the input voltage promoted SiC production (**Figure 2b**), due to a corresponding increase in the peak temperature during the flash cycle (between 500-3800 °C, **Figure S3-S4**). At ~1400°C, and equal mass of β-SiC and residual Si was obtained, whereas peak temperatures >2000 °C favored β-SiC with a maximum mass ratio of 10:1. Optimal SiC production occurred at 130 V and a corresponding peak temperature of ~2200 °C. Decreasing the proportion of c-Si mixed with CB from 2:1 wt% to 1:4 wt% had minimal effect on the resulting SiC content, which remained at ~ 92 wt% (**Figure 2c-d**); the observation that excess carbon did not facilitate the reaction may reflect the concomitant increase in sample volume and consequent non-uniform flash heating[49]. Repeated cycles of FJH slightly improved the β-SiC yield (**Figure 2e-f**), which increased to 95 wt% after 10 cycles, however, unreacted Si remained due to poor sample mixing that limited contact with CB. Regrinding the powder product in between each FJH cycle assisted the reaction between Si and CB, resulting in 99 wt% SiC after 10 cycles (**Figure S7**). β-SiC typically undergoes a crystal structure transformation to α-SiC at high temperature[27, 50], and indeed a new X-ray diffraction peak attributed to α-SiC emerged at 2θ = 38°[51]after 20 FJH cycles at 145 V (**Figure S8**), although β-SiC remained the dominant crystalline phase, probably due to limited mass-transport of Si and C atoms during the rapid Joule heating (ms to s timescale).

Raman vibrational spectroscopy of CB revealed peaks at 1335, 1576, and 2666 cm^{-1} (**Figure S9**) corresponding to the D, G, and 2D bands of graphitic carbon, respectively[35]. After a single FJH cycle, the carbon evidenced a higher IG:ID ratio, sharpening of the 2666 cm^{-1}, and the emergence of a new band ~2800 cm^{-1}, all indicative of enhanced graphitization (so-called 'flash graphene'). These changes were mirrored by XRD (**Figure S10**), wherein FJH sharpened and increased the intensity of the reflection at 2θ = 26°, associated with graphene. Note that extent of graphitization remained relatively low after FJH as the peak temperature achieved at 130 V was not optimal level for producing high-quality flash graphene[35].

Morphological analysis of FJH product indicates that most silicon carbide crystals are encapsulated by residual carbon, with only a small fraction exposed. EDS spectra also reveal a significantly higher carbon content. (**Figure S11**). Thermogravimetric analysis revealed that the product of a single FJH cycle contained ~26 wt% carbon (as flash graphene), that was removed by oxidation in an air atmosphere at 600 to 800° C (**Figure S12**). Two distinct SiC particle morphologies were observed in the FJH product after the removal of flash graphene by scanning electron microscopy (SEM, **Figure 3a, Figure S13**): polygonal prismatic crystals spanning 1-30 μm; and granular agglomerates formed from individual sub-particles spanning 100-400 nm[49]. Elemental mapping by energy dispersive spectroscopy (EDS) indicated a particle averaged composition of 47 atom% C, 49 atom% Si, and 3 atom% O (**Figure 3b-c**, note an intense peak is also visible from the Al SEM stub), and peaks associated with Ag and P residues from the parent photovoltaic cell wafers. The C:Si atomic ratio was almost stoichiometric for SiC; the small deviation may arise from residual unreacted Si, or trace oxidation of SiC to silica at the surface of particles. X-ray diffraction (XRD) of the product after oxidation of reactively-formed flash graphene revealed 99 % SiC (**Figure 3d**), consistent with the appearance of Raman peaks at 786 and 965 cm^{-1} characteristic of the transverse and longitudinal modes of β-SiC, respectively[52] (**Figure 3e**). As expected, the flash carbon content of the FJH product increased with c-Si:CB mass ratio, evidenced by an increasing mass loss after 20 min calcination at 700°C in air[27, 35] (**Figure S14**). Fourier transform infrared spectroscopy of the FJH product (FT-IR) confirmed a strong absorption peak at 820 cm^{-1} (**Figure S15**) corresponding to the Si-C vibration in β-SiC[53]. A broad, intense band at 3442 cm^{-1} is attributed to O-H stretch of physisorbed water, while a weaker band at ~1630 cm^{-1} is attributed to overlapping C=C and O-H vibrations[54, 55]. The weak band a ~1100 cm^{-1} is assigned to the Si-O stretch in SiO_2 arising from partial oxidation of the SiC surface[53, 56].

X-ray photoelectron spectroscopy (XPS) of the Si 2p core levels confirmed the presence of Si-C ($2p_{3/2}$ binding energy of 99.8 eV) and Si-O (102.4 eV binding energy) in a 2:1 molar ratio at the surface of the FJH product (**Figure 3f**, **Figure S16**). In addition to SiC, and the expected O 1s and 2s photoelectron peaks and O KLL Auger peak, trace Al and Ag were observed in the XP survey spectrum due to surface segregation of their metal oxides during calcination. As expected, the concentration of surface SiO_2 increased significantly post-calcination resulting in a fall in the SiC:SiO_2 molar ratio to 0.38 (**Figure S17a**). The C 1s XP spectrum of the FJH product (not shown) is dominated by an intense peak with an asymmetric lineshape at 284.7 eV characteristic of graphite[57], and a broad, higher binding energy peak 290.8 eV associated with $\pi \rightarrow \pi^*$ shake-up satellites from excitation of the aromatic network. Both carbon features are strongly attenuated post-calcination (**Figure S17b**) due to surface oxidation to alcohol/ether and carbonyl species with binding energies of 285.2 eV and 287.1 eV, respectively. These changes are also reflected in the surface elemental compositions:

View Article Online
DOI: 10.1039/D5EE01509J

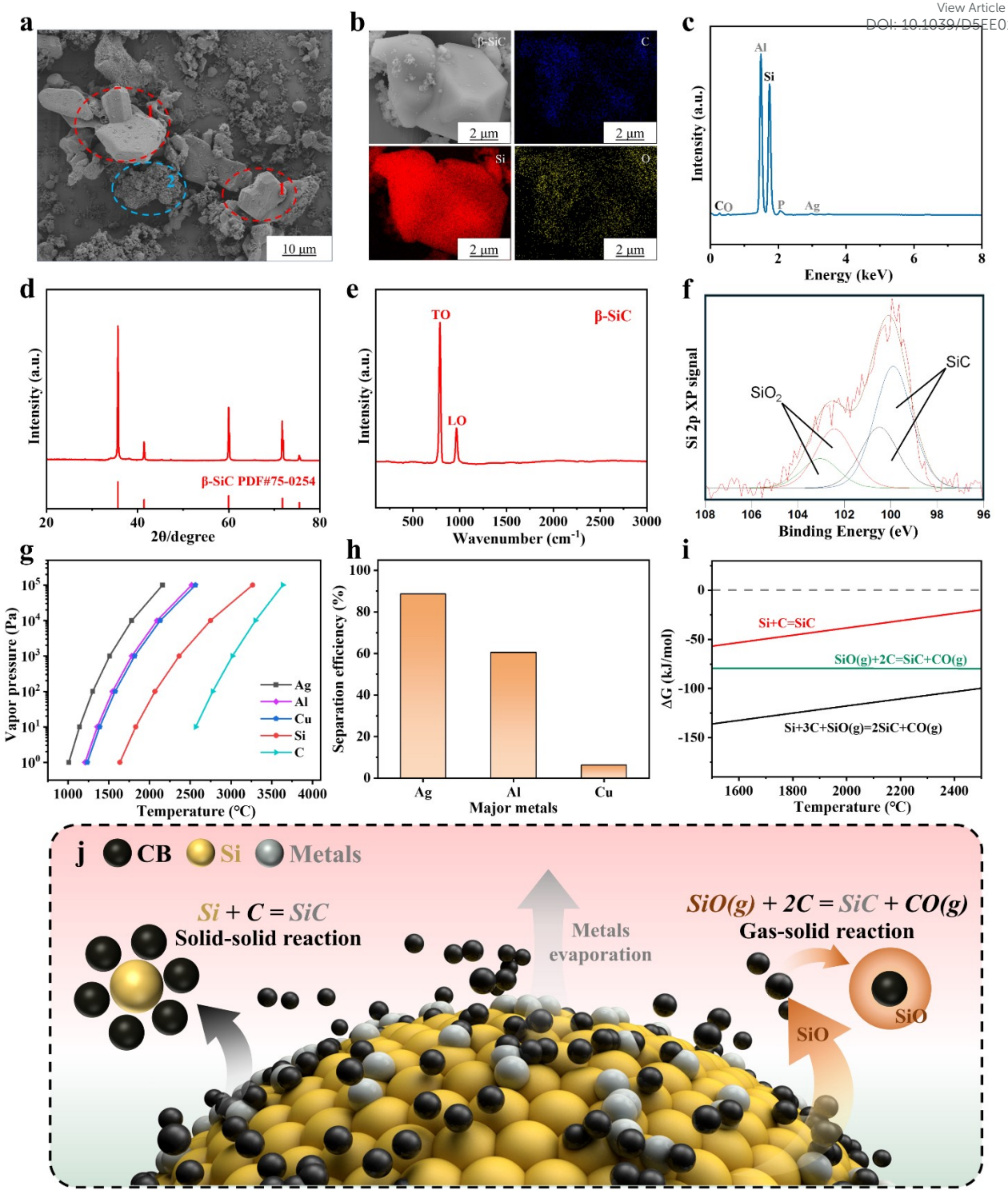

Figure 3 (a) SEM images of 10 cycles FJH product after 700 ℃ calcination for 20 min. (b) EDS elemental mapping, (c) EDS spectrum, (d) X-ray diffractogram, and (e) Raman spectrum of 10 cycles FJH product after 700 ℃ calcination for 20 min, and (f) Si 2p XP spectrum of 10 cycles FJH product pre-calcination. (g) Saturated vapor pressure versus temperature for metals in the parent c-Si powder. (h) Efficiency of metal removal from the c-Si/CB mixture after 10 FJH cycles. (i) Gibbs free energy changes versus temperature for possible reactions during FJH; dashed line indicates ΔG = 0. (j) Schematic of proposed reaction during FJH of waste c-Si.

the FJH product is carbon terminated with only trace Si (1.5 atom%) and oxygen (2.9 wt%), whereas post-calcination the surface carbon content fell to 35 atom% with balance being Si and O in a 2:1 atomic ratio (consistent with partial encapsulation of SiC nanoparticles by silica). Under controlled calcination temperature and time, direct calcination in air remains the most convenient way to purify the SiC in the flash-heated product[58-60].

The vapor pressure versus temperature relationship of metals identified in the parent crushed c-Si sample powder indicates that

View Article Online
DOI: 10.1039/D5EE01501J

an input voltage of 130 V (>2000 °C peak temperature) is sufficient to vaporize Ag, Al and Cu, enabling their in-situ light absorption in the PV module[63], that can itself react with carbon to form SiC during flash heating (Reaction 6) in a highly

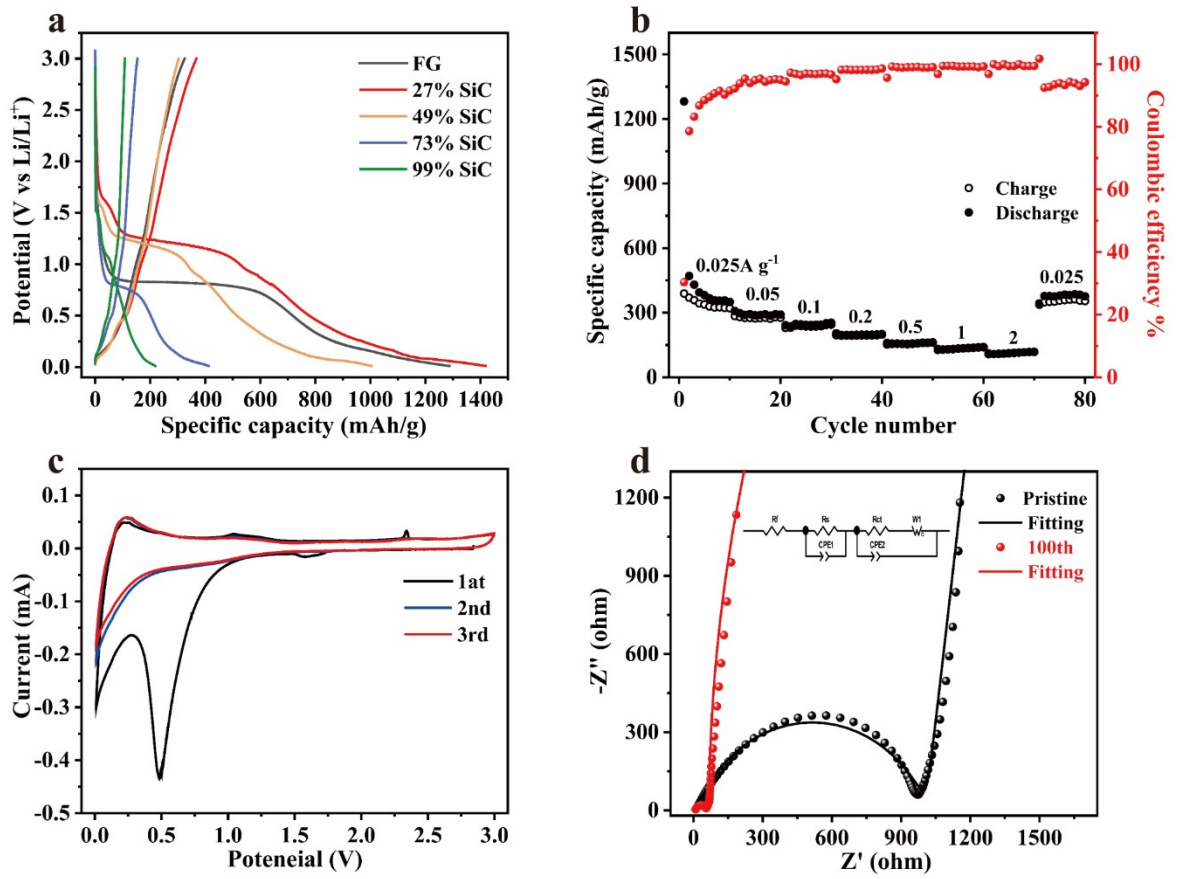

Figure 4 (a) First discharge/charge curves of SiC/FG composite anodes at 0.05 A g^{-1}. (b) Rate capacity of 27 wt% SiC composite anode at different current densities. (c) First three cyclic voltammagrams for 27 wt% SiC composite anode. (d) EIS spectra of SiC (27 wt% SiC/FG composite anode) before and after 100 cycles.

separation under the applied vacuum (1.3 kPa, **Figure 3g**). Inductively-coupled plasma optical emission spectroscopy (ICP-OES) confirmed a significant reduction in the content of these metals in the c-Si:CB mixture after a single cycle of FJH (**Figure S18**), representing 89 % and 61 % removal of Ag and Al, respectively (**Figure 3h**). Based on the above test data, the silicon-based yield by flash heating can reach 95% (**Text S3**).

Multiple, competing reactions may occur between c-Si and CB powders and residual O_2 during FJH in vacuo. At high temperature (>2500 °C), Si is prone to vaporization and/or diffusion into the carbon, albeit the solid-state reaction thus enabled to form SiC (Reaction 1) is only slightly exergonic (**Figure 3i**). In the presence of trace O_2, both Reactions 2 and 3 may occur (**Figure S19**), with the reactively-formed SiO gaseous product itself able to react with carbon alone (Reaction 4), or in combination with Si (Reaction 5), to yield SiC and CO. The latter of these solid-gas phase routes to SiC is slightly more exergonic, particularly <1800 °C, and likely the primary route to SiC in the FJH process[61]. We speculate that the two particle morphologies observed by SEM in the FJH product may arise from these different reaction pathways: Si+C resulting in larger crystals; $SiO_{(g)}$+C producing agglomerated, fluffy/porous particles[62]. The c-Si cells are often capped by a silicon nitride film to improve exergonic process <1800 °C (**Figure S19**).

$$Si+C=SiC \quad (1)$$

$$2C+O_2=2CO \quad (2)$$

$$2Si+O_2=SiO(g) \quad (3)$$

$$SiO(g)+2C=SiC+CO \quad (4)$$

$$Si+3C+SiO(g)=2SiC+CO \quad (5)$$

$$Si_3N_4(s)+3C=3SiC+2N_2 \quad (6)$$

3.2 FJH-derived SiC as an anode for lithium ion batteries

The FJH powder product contains SiC and flash graphene (FG), the latter of which is readily removed by high temperature calcination to yield high-purity SiC. We used pure FG obtained by flash Joule heating of CB, SiC obtained by FJH containing residual FG, and high-purity SiC after calcination of the FJH product, as anode materials in button batteries with lithium wafers as counter electrodes. Calcined SiC exhibited the lowest specific capacity, which increased with FG content due to increased carrier density and electrical conductivity [27] (**Figure S21**). An anode containing 27 % FJH produced SiC exhibited a higher specific capacity than pure FG (**Figure 4a**). The initial discharge-charge curves of different SiC/FG anodes at 0.05 A g^{-1}

current density evidenced a decrease in Coulombic efficiency with increasing FG content. The decrease in Coulombic efficiency is thus attributed to structural defects retained in the (partially graphitized) FG that are: (i) prone to react with the electrolyte during the initial charge/discharge cycle, and (ii) promote electrolyte physisorption; both factors increasing Li^+ ion consumption[64-66]. Optimizing the carbon source may further enhance the performance of such SiC composite anodes. After 80 cycles at different current densities, the 27 wt% SiC composite anode enabled stable cell recovery characteristics (**Figure 4b**). Cyclic voltammetry (CV) of the 27 wt% SiC composite (**Figure 4c**) showed significant evolution over three cycles spanning 0.01 V to 3.0 V (at 0.1 mV s^{-1}). A strong reduction peak at 0.5 V observed during the first cycle is attributed to irreversible reactions on the electrode surface, and resultant formation of the solid electrolyte interface (SEI) accompanied by a significant capacity loss[67, 68]. This reduction peak is absent in subsequent cycles, which exhibit almost identical I-V behaviour, indicating stabilization of the SEI[69, 70]. The small reduction peak at 1.7 V is likely due to irreversible lithium insertion into ultrafine pores of the FG[71, 72]. Small oxidation peaks at 0.25 V and 1.1 V are attributed to the de-intercalation of lithium ions from the FG and defective sites in the electrode, respectively[72, 73]. Weaker oxidation peaks between 2-3 V may be associated with heteroatoms at the electrode surface[67]. Electrochemical impedence spectroscopy (EIS) of the as-prepared 27 wt% SiC composite anode revealed a high frequency, semicircular region associated with charge transfer resistance (R_{ct}), and a low frequency, linear tail associated with lithium ion diffusion[68, 74] (**Figure 4e**). After 100 charge/discharge cycles at 0.05 A g^{-1}, the EIS curves showed a significant decrease in charge transfer resistance, as evidenced by the equivalent circuit fit with the Rct value decreasing from 997.4 Ω to 61.86 Ω. This is attributed to the formation of a stable SEI and concomitant faster Li^+ diffusion and charge transfer[75].

Life cycle assessment

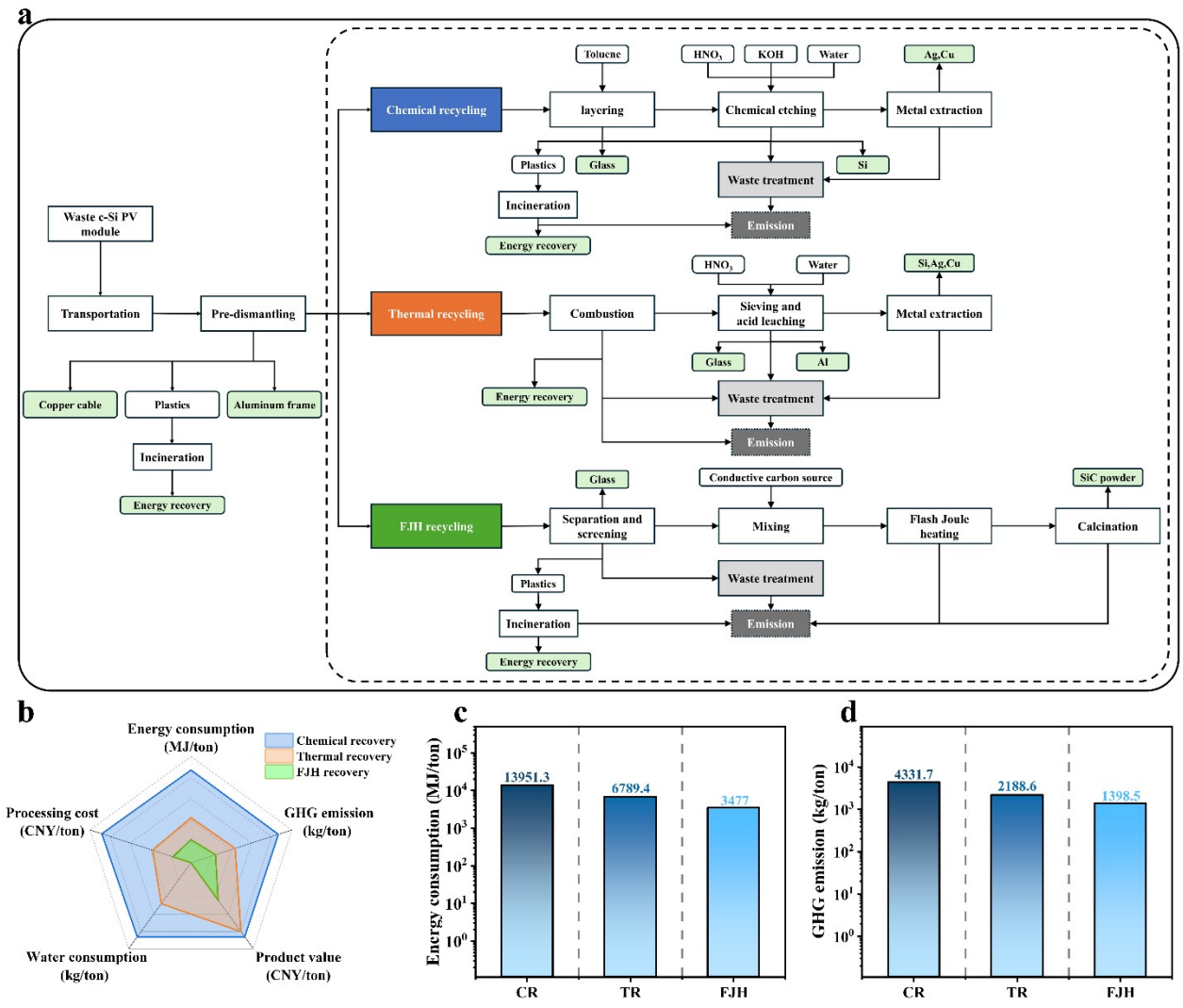

Figure 5 (a) Flowcharts of different waste PV recycling methods: chemical recycling (CR, blue), thermal recycling (TR, orange), and flash Joule heating recycling (FJH, green). (b) Process parameters for different waste PV recycling methods. Comparison of (c) energy consumption, and (d) GHG emissions for different recycling methods.

View Article Online DOI: 10.1039/D5EE01509J

A key enabler to the commercial application of FJH for recycling waste PV modules is scaling the amount of waste material that can be processed. FJH is highly scalable and can handle larger quantities of material by increasing the capacitance and input voltage of the equipment, and modifying auxiliary systems to enable continuous FJH processing with automated loading[35]. Environmental impacts of various recycling options were compared through a life cycle assessment (LCA) of FJH of one ton of waste PVmodules, alongside conventional chemical recycling (CR) and thermal recycling (TR)[19, 76] (**Figure 5a**) based on reported process flows[77-81]. The system boundary was defined by the input of raw materials (waste c-Si PV modules) and the output of recycled products and waste. Environmental impacts considered include energy and water consumption, and greenhouse gas (GHG) emissions (**Figure 5b**); further details are provided the Supporting Information and **Tables S2-S7**[82].

Waste photovoltaic modules are transported and subjected to pre-disassembly prior to integration into dedicated recycling processes. Energy recovery from the combustion of waste (such as backsheets, EVA and other plastics) is also considered, along with the treatment and emission of other solid waste and liquid waste. We estimate that recycling one ton of waste PV modules by FJH consumes 3477 MJ ton^{-1}, which is 75 % less than CR and 49 % less than TR (**Figure 5c**). Direct incineration and conventional recycling also generate substantial GHG emissions (**Figure 5d**) and consume large amounts of water, whereas FJH emits only 1398.5 kg of GHG ton^{-1} (68 % less than CR and 36 % less than TR). Most energy consumption and GHG emissions in FJH recycling arise during the separation and screening of waste PV modules. The FJH treatment itself accounts for only ~8.7 % of the total energy use and 7.6 % of total GHG emissions. Improved dismantling and separation processes could further reduce both energy consumption and GHG emissions. Compared to FJH, CR and TR involve more intensive treatment and management of solid and liquid waste, resulting in higher energy and material costs. The use of CB incurs significant material costs in FJH, which could be reduced by substituting recycled graphite, carbon fiber scraps or waste plastics as the source of conductive additives. This could reduce FJH costs to ~80 % and 53 % of those for CR and TR, respectively (**Figure S22**). While by-products of CR and TR include Si, Ag, Cu, and Al, these metals can also be recovered during FJH recycling for further separation, purification, and reuse, enhancing revenue potential. Although these metal impurities could be removed by chemical extraction prior to FJH of crushed Si cells, this would increase the materials inventory, and require the handling and subsequent neutralisation of strong mineral acids with attendant hazards and aqueous waste disposal. Pretreatment of Si wafers would thus have a significant negative impact on the life cycle assessment. In contrast, a benefit of FJH heating is that the high temperatures induced (that drive the chemical reaction between Si and C) vaporise the metal impurities allowing their rapid separation from SiC and downstream collection as solid metals. Although the market value of SiC is relatively low, the benefit-to-cost ratio of FJH recycling is 6.44, higher than that of both CR and TR, underscoring the technoeconomic feasibility of FJH for recycling waste c-Si PV modules.

In this work, we we process ~0.25 g of sample powder in a single batch experiment, however the transformation of waste PV modules into SiC powder is amenable to automation and continuous processing for scale-up (**Figure S23**). Additional LCA was performed to quantify energy consumption and GHG emissions at the 10 g and 100 g scales. Upscaling from mg to g of FJH product can be achieved by higher capacitance and voltage[27]. A ten-fold increase in the capacitance used in our experiments (to 0.9 F) and concomitant increase in the input voltage to 300 V should process of 10 g of sample with only a 33 % increase in energy consumption. Processing 100 g of sample would require capacitors to be substituted by a higher power (40 kW) electrical supply. From empirical data, energy consumption for 100 g of SiC would increase to 5 kWh.kg^{-1} (approximately a six-fold increase compared to that to produce 0.25 g, **Table S8**)[83]. Energy consumption, and in this instance GHG emissions from electrical power generation, thus scale non-linearly with the mass of reactant, and hence remain lower for FJH than CR and TR even at large scale.

Flash heating technologies will likely be extended to emerging perovskite and organic polymer PV cells, and have already proved valuable for the rapid fabrication of high efficiency, planar perovskite solar cells with the added benefit of eliminating the requirement for antisolvents[84]. Life cycle assessment indicates that flash (infrared) heating dramatically reduces the environmental impact and fabrication cost of perovskite active layers. Nanoporous PbI2 thin films (as percursors for organic–inorganic hybrid perovskites such as $CH_3NH_3PbI_3$) have also been printed by FJH[85]. High-quality inorganic halide perovskite thin-films can be prepared in a continuous fashion by flash sublimation of pre-mixed powders[86]. Inorganic perovskite powders may themselves be prepared by FJH[87, 88]. Flash (infrared) heating can also eliminate undesired defects in polycrystalline halide perovskite films, thereby improving optoelectrical performance[89]. We envisage that FJH could be applied to recover metal elements (Pb, Cs, Rb) from spent inorganic perovskite PV units with a high energy efficiency. The use of FJH in preparing carbon-based energy materials was recently reviewed[90]; we envisage that conjugated polymers in OPV devices could serve as a source of flash graphene for producing SiC (as in this work) or in alternative energy applications.

Conclusions

The effectiveness of FJH to produce high-purity SiC through recycling c-Si PV cells in the presence of conductive carbon is demonstrated. The SiC yield is sensitive to applied potential and hence peak temperature during flash heating cycles, but less sensitive to the amount of blended carbon black or number of flash heating cycles. High purity SiC (98 %) is readily obtained following FJH of a 1:1 mass ratio of crushed c-Si and carbon black at 130 V, and subsequent calcination at 700 °C under air to remove residual ‘flash graphene’, representing a Si recovery rate of 95 %. The composite product of SiC and flash graphene prepared from FJH shows potential as a lithium battery anode and could be a candidate for applications in ceramics and

reinforced composites, pending further investigation. Life cycle assessment of a FJH process for recycling waste c-Si PV cells to yield SiC revealed significant environmental and cost advantages compared to chemical or thermal recycling, notable in reduced energy consumption and CO_2 emissions. FJH may also prove an innovative technology for converting other Si containing wastestreams into SiC, provided that process automation and continuous manufacturing can be integrated to facilitate scale-up.

Conflicts of interest

There are no conflicts to declare.

Data availability

All data supporting the findings of this study are provided in the main text and Supplementary Information. Additional raw data are available from the corresponding author [F.G.] upon reasonable request.

Acknowledgements

All data supporting the findings of this study are provided in the main text and Supplementary Information. Additional raw data are available from the corresponding author [F.G.] upon reasonable request.

References

1 P. Nain and A. Kumar, *J. Clean Prod.*, 2022, **343**, 14.
2 B. Al Zaabi and A. Ghosh, *Sol Energy*, 2024, **283**, 13.
3 J. Prime, I. A. Ahmed, D. Akande, N. Elhassan, G. Escamilla, A. Jamdade, Y. Melnikov and A. Whiteman, *Renewable energy statistics 2024*, International Renewable Energy Agency, Abu Dhabi, 2024.
4 M. S. Chowdhury, K. S. Rahman, T. Chowdhury, N. Nuthammachot, K. Techato, M. Akhtaruzzaman, S. K. Tiong, K. Sopian and N. Amin, *Energy Strateg. Rev.*, 2020, **27**, 11.
5 S. K. Venkatachary, R. Samikannu, S. Murugesan, N. R. Dasari and R. U. Subramaniyam, *Environ. Technol. Innov.*, 2020, **20**, 14.
6 Y. Xu, J. H. Li, Q. Y. Tan, A. L. Peters and C. R. Yang, *Waste Manage.*, 2018, **75**, 450-458.
7 X. T. Wang, J. G. Xue and X. L. Hou, *Renew. Energy*, 2023, **214**, 39-54.
8 C. L. Zhou, N. Bai, B. J. An and J. Li, *Sol. Energy Mater. Sol. Cells*, 2025, **283**, 9.
9 R. J. Guo, D. Han, W. Chen, L. J. Dai, K. Y. Ji, Q. Xiong, S. S. Li, L. K. Reb, M. A. Scheel, S. Pratap, N. Li, S. S. Yin, T. X. Xiao, S. Z. Liang, A. L. Oechsle, C. L. Weindl, M. Schwartzkopf, H. Ebert, P. Gao, K. Wang, M. J. Yuan, N. C. Greenham, S. D. Stranks, S. V. Roth, R. H. Friend and P. Müller-Buschbaum, *Nat. Energy*, 2021, **6**, 977-+.
10 X. Song, K. Zhang, R. J. Guo, K. Sun, Z. X. Zhou, S. L. Huang, L. Huber, M. Reus, J. G. Zhou, M. Schwartzkopf, S. Roth, W. Z. Liu, Y. Liu, W. G. Zhu and P. Müller-Buschbaum, *Adv. Mater.*, 2022, **34**, 12.
11 R. Vinayagamoorthi, P. B. Bhargav, N. Ahmed, C. Balaji, K. Aravinth, A. Krishnan, R. Govindaraj and P. Ramasamy, *J. Environ. Chem. Eng.*, 2024, **12**, 22.
12 J. Pastuszak and P. Wegierek, *Materials*, 2022, **15**, 30.
13 G. H. Yan, M. R. Zhang, Z. S. Sun, P. F. Zhao and B. Zhang, *Energ Source Part A*, 2023, **45**, 10890-10908.
14 Y. K. Yi, H. S. Kim, T. Tran, S. K. Hong and M. J. Kim, *J. Air Waste Manage. Assoc.*, 2014, **64**, 797-807.
15 R. Deng, Y. T. Zhuo and Y. S. Shen, *Resour. Conserv. Recycl.*, 2022, **187**, 15.
16 J. I. Kwak, S. H. Nam, L. Kim and Y. J. An, *J. Hazard. Mater.*, 2020, **392**, 13.
17 T. Maani, I. Celik, M. J. Heben, R. J. Ellingson and D. Apul, *Sci. Total Environ.*, 2020, **735**, 11.
18 Z. N. Ndalloka, H. V. Nair, S. Alpert and C. Schmid, *Sol Energy*, 2024, **270**, 112379.
19 J. Wang, Y. Feng and Y. Q. He, *Sol. Energy Mater. Sol. Cells*, 2024, **270**, 13.
20 G. Granata, F. Pagnanelli, E. Moscardini, T. Havlik and L. Toro, *Sol. Energy Mater. Sol. Cells*, 2014, **123**, 239-248.
21 L. G. Zhang and Z. M. Xu, *Environ. Sci. Technol.*, 2016, **50**, 9242-9250.
22 S. Kang, S. Yoo, J. Lee, B. Boo and H. Ryu, *Renew. Energy*, 2012, **47**, 152-159.
23 M. F. Azeumo, C. Germana, N. M. Ippolito, M. Franco, P. Luigi and S. Settimio, *Sol. Energy Mater. Sol. Cells*, 2019, **193**, 314-319.
24 H. Akram Cheema, S. Ilyas, H. Kang and H. Kim, *Waste Manag*, 2024, **174**, 187-202.
25 F. Padoan, P. Altimari and F. Pagnanelli, *Sol Energy*, 2019, **177**, 746-761.
26 R. Q. Ma, J. H. Shi, W. X. Lin and J. J. Chen, *Mater. Chem. Phys.*, 2020, **253**, 6.
27 Y. Cheng, J. H. Chen, B. Deng, W. Y. Chen, K. J. Silva, L. Eddy, G. Wu, Y. Chen, B. W. Li, C. Kittrell, S. C. Xu, T. D. Si, A. A. Marti, B. I. Yakobson, Y. F. Zhao and J. M. Tour, *Nat. Sustain.*, 2024, **7**, 14.
28 I. D. Booker, I. Farkas, I. G. Ivanov, J. u. Hassan and E. Janzén, *Physica B: Condensed Matter*, 2016, **480**, 23-25.
29 Y. Yang, Z. M. Lin and J. T. Li, *J. Eur. Ceram. Soc.*, 2009, **29**, 175-180.
30 X. Z. Guo, L. Zhu, W. Y. Li and H. Yang, *J Adv Ceram*, 2013, **2**, 128-134.
31 A. Griffin, M. Robertson, Z. Gunter, A. Coronado, Y. Z. Xiang and Z. Qiang, *Ind. Eng. Chem. Res.*, 2024, **63**, 19398-19417.
32 K. J. Silva, K. M. Wyss, C. H. Teng, Y. Cheng, L. J. Eddy and J. M. Tour, *Small*, 2024, DOI: 10.1002/smll.202311021, 8.
33 P. A. Advincula, W. Meng, J. L. Beckham, S. Nagarajaiah and J. M. Tour, *Macromolecular Materials and Engineering*, 2023, **309**, 2300266.
34 W. A. Algozeeb, P. E. Savas, D. X. Luong, W. Y. Chen, C. Kittrell, M. Bhat, R. Shahsavari and J. M. Tour, *ACS Nano*, 2020, **14**, 15595-15604.
35 D. X. Luong, K. V. Bets, W. A. Algozeeb, M. G. Stanford, C. Kittrell, W. Chen, R. V. Salvatierra, M. Ren, E. A. McHugh, P. A. Advincula, Z. Wang, M. Bhatt, H. Guo, V. Mancevski, R. Shahsavari, B. I. Yakobson and J. M. Tour, *Nature*, 2020, **577**, 647-651.
36 K. M. Wyss, R. D. De Kleine, R. L. Couvreur, A. Kiziltas, D. F. Mielewski and J. M. Tour, *Communications Engineering*, 2022, **1**, 3.
37 B. Deng, D. X. Luong, Z. Wang, C. Kittrell, E. A. McHugh and J. M. Tour, *Nat. Commun.*, 2021, **12**, 8.
38 C. Jia, L. M. Sun, X. Wu, F. B. Yu, L. T. Lin, Z. L. He, J. Gao, S. C. Zhang and X. D. Zhu, *ACS ES&T Eng.*, 2024, **4**, 938-946.
39 Y. C. Yin, C. Li, X. S. Hu, D. X. Zuo, L. Yang, L. H. Zhou, J. L. Yang and J. Y. Wan, *ACS Energy Lett.*, 2023, **8**, 3005-3012.
40 R. B. Wu, K. Zhou, C. Y. Yue, J. Wei and Y. Pan, *Prog. Mater. Sci.*, 2015, **72**, 1-60.
41 S. N. Perevislov, M. V. Tomkovich, A. S. Lysenkov and M. G. Frolova, *Refract. Ind. Ceram.*, 2019, **59**, 534-544.

42 F. Wang, L. Cheng, Y. Xie, J. Jian and L. Zhang, *J. Alloy. Compd.*, 2015, **625**, 1-7.
43 J. X. Dai, J. J. Sha, Z. F. Zhang, Y. C. Wang and W. Krenkel, *Ceram. Int.*, 2015, **41**, 9637-9641.
44 R. B. Wu, K. Zhou, X. K. Qian, J. Wei, Y. Tao, C. H. Sow, L. Y. Wang and Y. Z. Huang, *Mater. Lett.*, 2013, **91**, 220-223.
45 X. P. Li, Z. Q. Li, L. K. Que, Y. J. Ma, L. Zhu and C. H. Pei, *J. Alloy. Compd.*, 2020, **835**, 12.
46 E. A. Belenkov, E. N. Agalyamova and V. A. Greshnyakov, *Phys. Solid State*, 2012, **54**, 433-440.
47 V. V. Pujar and J. D. Cawley, *Journal of the American Ceramic Society*, 1995, **78**, 774-782.
48 Y. Y. Wang, S. Dong, X. T. Li, C. Q. Hong and X. H. Zhang, *Ceram. Int.*, 2022, **48**, 8882-8913.
49 A. A. Lavrenchuk, M. Y. Speranskiy, A. Y. Pak, A. P. Korchagina and A. V. Vlasov, *J. Alloy. Compd.*, 2024, **1003**, 7.
50 W. S. Y. Woo Sik Yoo and H. M. Hiroyuki Matsunami, *Japanese Journal of Applied Physics*, 1991, **30**, 545.
51 Y. J. Zhao, Y. N. Zhang, C. R. Yang and L. F. Cheng, *Carbon*, 2021, **171**, 474-483.
52 P. Rai, J. S. Park, G. G. Park, W. M. Lee, Y. T. Yu, S. K. Kang, S. Y. Moon and B. G. Hong, *Adv. Powder Technol.*, 2014, **25**, 640-646.
53 M. Yu, E. Temeche, S. Indris and R. M. Laine, *Green Chemistry*, 2021, **23**, 7751-7762.
54 Q. Wang, Y. Li, S. Jin, S. Sang, Y. Xu, G. Wang and X. Xu, *Ceram. Int.*, 2017, **43**, 13282-13289.
55 J. H. Cha, H. H. Choi, Y. G. Jung, S. C. Choi and G. S. An, *Ceram. Int.*, 2020, **46**, 14384-14390.
56 G. Y. Yang, R. B. Wu, Y. Pan, J. J. Chen, R. Zhai, L. L. Wu and J. Lin, *Physica E*, 2007, **39**, 171-174.
57 R. I. R. Blyth, H. Buqa, F. P. Netzer, M. G. Ramsey, J. O. Besenhard, P. Golob and M. Winter, *Appl. Surf. Sci.*, 2000, **167**, 99-106.
58 H. A. Bland, E. L. H. Thomas, G. M. Klemencic, S. Mandal, D. J. Morgan, A. Papageorgiou, T. G. Jones and O. A. Williams, *Sci Rep*, 2019, **9**, 9.
59 A. Kaur, P. Chahal and T. Hogan, *IEEE Electron Device Lett.*, 2016, **37**, 142-145.
60 Z. D. Jiang, C. X. Zhang, X. X. Qu, B. L. Xing, G. X. Huang, B. Xu, C. L. Shi, W. W. Kang, J. Yu and S. W. Hong, *Electrochim. Acta*, 2021, **372**, 11.
61 S. Larpkiattaworn, P. Ngernchuklin, W. Khongwong, N. Pankurddee and S. Wada, *Ceram. Int.*, 2006, **32**, 899-904.
62 R. Dhiman, E. Johnson, E. M. Skou, P. Morgen and S. M. Andersen, *J. Mater. Chem. A*, 2013, **1**, 6030-6036.
63 G. H. Liu, K. Yang, J. T. Li, K. Yang, J. S. Du and X. Y. Hou, *J. Phys. Chem. C*, 2008, **112**, 6285-6292.
64 H. L. Chen, Y. Wang, D. C. Meng, Y. Y. Zhu, Y. S. He, Z. F. Ma and L. S. Li, *Small*, 2024, **20**, 9.
65 M. Reynaud, J. Serrano-Sevillano and M. Casas-Cabanas, *Chem. Mat.*, 2023, **35**, 3345-3363.
66 A. D. de Limé, T. Lein, S. Maletti, K. Schmal, S. Reuber, C. Heubner and A. Michaelis, *Batteries Supercaps*, 2022, **5**, 18.
67 Y. Q. Zhang, Q. Ma, S. L. Wang, X. Liu and L. Li, *ACS Nano*, 2018, **12**, 4824-4834.
68 D. X. Liu, X. Qu, B. L. Zhang, J. J. Zhao, H. W. Xie and H. Y. Yin, *ACS Sustain. Chem. Eng.*, 2022, **10**, 5739-5747.
69 F. Yang, P. C. Deng, H. He, R. L. Hong, K. Xiang, Y. Cao, B. B. Yu, Z. M. Xie, J. M. Lu, Z. K. Liu, D. Khan, D. Harbottle, Z. H. Xu, Q. X. Liu and Z. G. Tang, *Chem. Eng. J.*, 2024, **494**, 11.
70 H. Y. Yang, L. J. Sun, S. L. Zhai, X. Wang, C. C. Liu, H. Wu and W. Q. Deng, *ACS Appl. Nano Mater.*, 2023, **6**, 2450-2458.
71 S. Z. Huang, J. Y. Wang, Z. Y. Pan, J. L. Zhu and P. K. Shen, *J. Mater. Chem. A*, 2017, **5**, 7595-7602.
72 B. K. Guo, X. Q. Wang, P. F. Fulvio, M. F. Chi, S. M. Mahurin, X. G. Sun and S. Dai, *Adv. Mater.*, 2011, **23**, 4661-+.
73 Z. Shang, Z. Naizhe, Z. W. Ying, D. J. Zou, F. Dai, J. H. Xie, J. Shao, X. G. Liu and S. M. Xu, *Chem. Eng. J.*, 2025, **505**, 10.
74 C. F. Liu, Z. Neale, J. Q. Zheng, X. X. Jia, J. J. Huang, M. Y. Yan, M. Tian, M. S. Wang, J. H. Yang and G. Z. Cao, *Energy Environ. Sci.*, 2019, **12**, 2273-2285.
75 W. C. Bi, G. H. Gao, G. M. Wu, M. Atif, M. S. AlSalhi and G. Z. Cao, *Energy Storage Mater.*, 2021, **40**, 209-218.
76 J. Li, J. L. Shao, X. L. Yao and J. S. Li, *Resour. Conserv. Recycl.*, 2023, **196**, 11.
77 P. Dias, L. Schmidt, M. M. Lunardi, N. L. Chang, G. Spier, R. Corkish and H. Veit, *Resour. Conserv. Recycl.*, 2021, **165**, 14.
78 C. E. L. Latunussa, F. Ardente, G. A. Blengini and L. Mancini, *Sol. Energy Mater. Sol. Cells*, 2016, **156**, 101-111.
79 F. Ardente, C. E. L. Latunussa and G. A. Blengini, *Waste Manage.*, 2019, **91**, 156-167.
80 F. Corcelli, M. Ripa, E. Leccisi, V. Cigolotti, V. Fiandra, G. Graditi, L. Sannino, M. Tammaro and S. Ulgiati, *Ecol. Indic.*, 2018, **94**, 37-51.
81 J. Park, W. Kim, N. Cho, H. Lee and N. Park, *Green Chemistry*, 2016, **18**, 1706-1714.
82 D. Mao, S. Q. Yang, L. Ma, W. H. Ma, Z. Q. Yu, F. S. Xi and J. Yu, *J. Clean Prod.*, 2024, **434**, 16.
83 D.-N. Wu, J. Sheng, H.-G. Lu, S.-D. Li and Y. Li, *ChemRxiv*, 2024, preprint, DOI: 10.26434/chemrxiv-2024-0c0lk.
84 S. Sánchez, M. Vallés-Pelarda, J. A. Alberola-Borràs, R. Vidal, J. J. Jerónimo-Rendón, M. Saliba, P. P. Boix and I. Mora-Seró, *Mater. Today*, 2019, **31**, 39-46.
85 H. M. Wei, X. Y. Zhao, Y. Wei, H. Ma, D. Q. Li, G. Chen, H. Lin, S. S. Fan and K. L. Jiang, *NPG Asia Mater.*, 2017, **9**, 8.
86 T. Abzieher, C. P. Muzzillo, M. Mirzokarimov, G. Lahti, W. F. Kau, D. M. Kroupa, S. G. Cira, H. W. Hillhouse, A. R. Kirmani, J. Schall, D. Kern, J. M. Luther and D. T. Moore, *J. Mater. Chem. A*, 2024, **12**, 8405-8419.
87 L. Y. Zheng, A. Nozariasbmarz, Y. C. Hou, J. Yoon, W. J. Li, Y. Zhang, H. D. Wu, D. Yang, T. Ye, M. Sanghadasa, K. Wang, B. Poudel, S. Priya and K. Wang, *Nat. Commun.*, 2022, **13**, 13.
88 K. W. Wang, B. S. Ma, T. Li, C. X. Xie, Z. Z. Sun, D. G. Liu, J. L. Liu and L. N. An, *Ceram. Int.*, 2020, **46**, 18358-18361.
89 P. Serafini, P. P. Boix, E. M. Barea, T. Edvinson, S. Sánchez and I. Mora-Seró, *Sol. RRL*, 2023, **7**, 2.
90 J. H. Yuan, Y. Z. Zhang, F. Z. Chen and Z. R. Gu, *J. Mater. Chem. C*, 2024, **12**, 14729-14753.

View Article Online
DOI: 10.1039/D5EE01509J

Data Availability Statement

All data supporting the findings of this study are provided in the main text and Supplementary Information. Additional raw data are available from the corresponding author [F.G.] upon reasonable request.